Received: 4 February 2018 | Revised: 2 April 2018 | Accepted: 11 April 2018

DOI: 10.1002/apj.2202

RESEARCH ARTICLE

WILEY Asia-Pacific Journal of Chemical Engineering | Curtin University

A novel passive micromixer with modified asymmetric lateral wall structures

Hanlin Wang[1] | Liuyong Shi[1] | Teng Zhou[1] | Chao Xu[2] | Yongbo Deng[3]

[1]Mechanical and Electrical Engineering College, Hainan University, Haikou 570228 Hainan, China

[2]State Key Laboratory of Industrial Control Technology and Institute of Cyber-Systems and Control, Zhejiang University, Hangzhou 310027 Zhejiang, China

[3]State Key Laboratory of Applied Optics, Changchun Institute of Optics, Fine Mechanics and Physics (CIOMP), Chinese Academy of Science, Changchun 130033 Jilin, China

Correspondence
Liuyong Shi and Teng Zhou, Mechanical and Electrical Engineering College, Hainan University, Haikou, 570228 Hainan, China.
Email: shiliuyong@hainu.edu.cn; zhouteng@hainu.edu.cn

Yongbo Deng, State Key Laboratory of Applied Optics, Changchun Institute of Optics, Fine Mechanics and Physics (CIOMP), Chinese Academy of Science, Changchun, 130033 Jilin, China.
Email: dengyb@ciomp.ac.cn

Funding information
Open Research Project of the State Key Laboratory of Industrial Control Technology, Grant/Award Number: ICT170295; Youth Fund of Hainan University, Grant/Award Numbers: hdkyxj201722 and hdkyxj201721; National Natural Science Foundation of China, Grant/Award Number: 51605124

Abstract

Homogeneous and rapid mixing in microfluidic devices have always been the premise requirement due to its integration with bioengineering and chemical experiments. In this work, a novel passive micromixer with modified asymmetric lateral wall structures is designed. The numerical simulation is carried out at the Reynolds number ranging from 0.1 to 100 for the novel microchannel and the ordinary "S"-shaped microchannel. The results indicate that, compared with the "S"-shaped micromixer, the novel structure exhibits superior mixing performance, which can be attributed to the increasing inertial effect and formation of secondary flow. The simulation results suggest that the novel micromixer developed here will achieve an efficient mixing performance.

KEYWORDS

lateral structure, microfluidics, numerical simulations, passive micromixer, secondary flow

1 | INTRODUCTION

Microfluidics is developing rapidly owing to its tremendous potential in lab-on-a-chip.[1] Bioengineering and chemical experiment have been integrated gradually with microfluidics for pursuit of the species operation efficiently, such as hybrid analysis of reagents, chemical reaction,[2] and the mixing and separation of particle.[3-5] As a core component of the microfluidic system,[6,7] the micromixer with a well-designed structure plays an

imperative role of mixing two or more samples in microchannel. According to those recent research works, the micromixer can be divided into two types: active micromixer and passive micromixer.[8-10]

The active micromixer requires loading an external source for disturbance of flow field to achieve a better mixing effect.[11-17] Its composition is varied and complicated relatively, usually including microelectrodes and sensitive magnet microdetector into chips. Accordingly, the active micromixer will be destined to meet some complex difficulties to overcome during multiple design, development, and production process.[18-24] Compared with the active micromixer, the passive micromixer demands a much easier manufacturing condition because it does not require external energy for hydrodynamic driving control.[25-30] Passive mixing behavior typically relies on diversified microchannel structural design for fluid flow guiding along the wall and distortion to obtain the desired mixing performance.[31-34] Hence, the improvement and optimization of the passive micromixer structure have always been the focus of research; a variety of passive micromixers with diverse structures have been implemented.[34-42]

In order to design a unique microfluidic channel for improving its mixing performance of the passive micromixer,[43-46] we employ the finite element method to establish a novel passive micromixer with modified asymmetric lateral structures. The elaborated structure compels the fluid flow along its converging–diverging channels, and mixing degree of fluid can be promoted by interacting behavior among fluid elements, which can be evaluated by mixing index M.[47-49] The velocity profiles perpendicular to the axis of the microchannel will be introduced to illuminate the mixing behavior in species under varying Reynolds numbers.[50,51] Through a mass of significative numerical simulations, the fluid velocity field and the concentration distribution under various Reynolds numbers are illustrated. The results based on computational fluid dynamics method have been proven with high reliability in the qualitative analysis and quantitative calculation of fluid behavior. Ultimately, the passive micromixer with modified asymmetric lateral wall structures is achieved.

2 | METHODOLOGY

2.1 | Mathematical model

The fluid momentum equation of an incompressible Newtonian liquid in micromixers and the continuity equation are described as follows:

$$\rho(\mathbf{u}\cdot\nabla)\mathbf{u} = -\nabla p + \nabla\cdot\eta\left(\nabla\mathbf{u} + (\nabla\mathbf{u})^T\right), \tag{1}$$

$$-\nabla\cdot\mathbf{u}=0, \tag{2}$$

where $\mathbf{u}$ is the velocity of fluid, ρ is the fluidic density, p is the fluidic pressure, and η is the fluidic viscosity.

For the purpose of tracking the location of the interface between the two fluids, convection–diffusion equation is usually used to numerically solve the concentration field.

$$\frac{\partial c}{\partial t} + (\mathbf{u}\cdot\nabla)c = D\nabla^2 c, \tag{3}$$

where c and D are concentration and diffusion coefficient of the species, respectively. For the steady convection–diffusion equation, the concentrations at inlets are assigned as

$$c = 0\ \mathrm{mol/m^3} \quad \text{at } \Gamma_{\text{inlet1}},$$

$$c = 1\ \mathrm{mol/m^3} \quad \text{at } \Gamma_{\text{inlet2}}.$$

And the boundary conditions are

$$u = u_0 \ \text{ at } \Gamma_{\text{inlet}},$$

$$u = 0 \quad \text{at } \Gamma_{\text{wall}},$$

$$p = 0,$$

$$\eta\left(\nabla\mathbf{u} + (\nabla\mathbf{u})^T\right)\mathbf{n}=0 \quad \text{at } \Gamma_{\text{outlet}}.$$

There is an important nondimensional number named Re, which represents the ratio of inertia force and viscous force, and it can be expressed as

$$\mathrm{Re} = \frac{uL\rho}{\eta}. \tag{5}$$

In order to investigate the efficiency of the micromixer, the mixing degree of the species can be evaluated by a variable index, which is defined as

$$M = 1-\sqrt{\frac{1}{N}\sum_{i=1}^{N}\left(\frac{c_i-\bar{c}}{\bar{c}}\right)^2}, \tag{6}$$

where M is the mixing efficiency, N is the total number of sampling points, c_i is the normalized concentration at the sampling point, and $\bar{c}$ is the expected normalized concentration. The mixing efficiency M ranges from 0 to 1("0"

and "1" donate the species unmixed and full mixed, respectively). The higher M value indicates the more homogeneous concentration distribution and the better mixing performance.

2.2 | Numerical method

The schematic diagram of the two-dimensional structure of the designed micromixer is shown in Figure 1, and its main parameters are exhibited in Table 1. Different from the ordinary "S"-shaped structures, only one side of semicircular pipe is modified to straight wall structures; in other words, the lateral straight wall structures are integrated together with the straight path with an asymmetrical array. Although the fluid flows along with the asymmetry lateral channel, it will be induced to accelerate due to decreasing cross-sectional area of straight wall structures, like a converging channel, and then the fluid will move from the current export of lateral channel to the next substructure periodically.

The commercial finite element package COMSOL Multiphysics (version 5.3) is used to carry out the three-dimensional simulation of the micromixer. This software can couple many useful physical modules smoothly for computational fluid dynamics. The simulation model of this study is made up of two classic physical modules, the laminar flow and the transport of diluted species. Our main works focus on the improvement of mixing performance of the designed microchannel with asymmetric lateral wall structures. The elaborated discussion about the mixing level will be carried out in the next section.

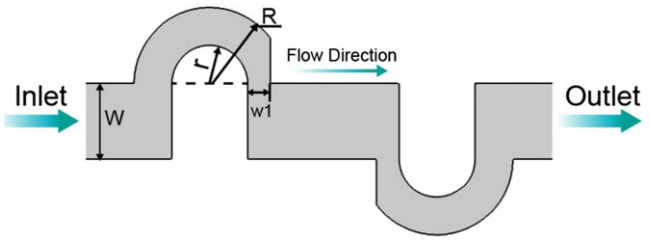

FIGURE 1 The schematic diagram of two-dimensional structure of the micromixer with asymmetric lateral wall structures

TABLE 1 Dimensions of micromixer

Parameter	Value (μm)	Parameter	Value (μm)
W	100	R	100
w1	30	r	50

3 | RESULTS AND DISCUSSION

This section is divided into the following two parts. The first part is the model discussion, such as the independent grid system in the model, and the analysis of the mixing mechanism based on the calculation results of the flow field in the channel. The other part is based on numerical calculation of concentration distribution, such as vortex formation distribution and final mixing efficiency in outlet.

3.1 | Results of the simulation and mixing mechanism

In order to show the construction of the micromixer more intuitively, we expand the plane shown in Figure 1 to the three-dimensional simulation model by using COMSOL Multiphysics software, as shown in Figure 2. In this model, the density of the fluid is 1×10^3 kg/m^3, the dynamic viscosity of the fluid is 1×10^{-3} Pa·s, and the diffusion coefficient is chosen as 10^{-9} m^2/s. It is clear that the micromixer consists of two inlets and one outlet; the width of channel is 100 μm.

For ensuring the accuracy of numerical calculation, we develop several grid independent of solutions to establish the model; the number of grids ranges from 25,094 to 333,676 for detailed testing. The local velocity profile along the middle line at the outlet is shown in Figure 3 a; here, we compared the local velocity profile with four mesh refinements under Re = 10. Thus, we chose the 206,388 as a number of independent grid elements because it can ensure adequate accuracy and save of numerical computation time at the same time. Figure 3 b shows the mesh system with 206,388 elements of independent grid; the maximum element size and the minimum element size are 8.81 and 0.952 μm, respectively. Based on the data statistics in COMSOL 5.3, the minimum element quality and the average unit quality can reach 0.25 and 0.88, respectively, in the structure of micromixer. According to finite element method, we can be convinced that the solution and analysis of the model under the grid system are accurate and reliable enough.

For contrast, we set up two kinds of three-dimensional micromixer models to highlight the advantage of novel micromixer in mixing efficiency; one is ordinary "S"-shaped structure, the other is the microchannel with modified lateral wall structure, and the both are shown in Figure 4.

For a further intuitive presentation, we select different Reynolds numbers (Re = 1, 50, 100) to demonstrate the mixing results as shown in Figure 5. The numerical

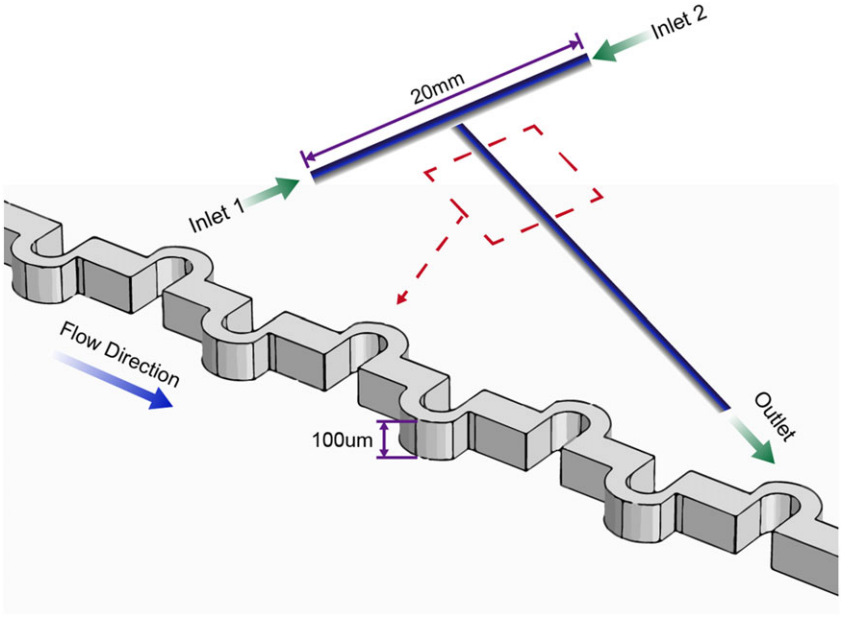

FIGURE 2 The schematic diagram of the three-dimensional microchannel

results in microchannel with normal "S" shape under three kinds of Reynolds number are presented in Figure 5a–c; similarly, the numerical results in microchannel with modified asymmetric lateral wall structures are displayed in Figure 5d–f.

Based on the observation of fluid flow in micromixer in general, two kinds of species from the entrance synchronously flow in parallel through the initial straight microchannel, then turn into the narrow flow runner due to the reduced cross-sectional area of the lateral wall structure. Along with the internal lateral wall structure curves, fluid flow behavior is changed under the restraint of bending lateral wall; thus, the centrifugal force is generated. Further, the radial pressure gradient is formed, and the fluid motion could be promoted due to the effect of inertia on the semicircle structure of lateral wall, so the fluid velocity in the curved path will be accelerated dramatically. At this time, the differentiation can be distinguished between two kinds of micromixer; the fluid velocity in modified lateral wall structure (shown in Figure 5d–f) is higher significantly than that in the ordinary "S"-shaped microchannel (shown in Figure 5a–c), which can be attributed to its designed unique lateral wall structure impelling the fluid movement through a narrower path. Moreover, because the lateral walls in the micromixer own an arrangement with the asymmetrical distribution on either side along the straight channel, it can also create nonuniformity of fluid flow, which means that more disturbance occurred between the reagents may be induced into flow field. Soon afterward, the fluid flows from the lateral structure into the straight path, and the flow direction perpendicular to the axis of the rectangle microchannel will be shifted when it encounters the wall boundary, which forces the fluid into two strands moving to the upper and lower walls, respectively, at the vertical plane as shown in Figure 5. Herein, the vortices will be generated with the symmetric distribution, namely, as the secondary flow.

It is universally known that the mixing of reagents at low Reynolds number mainly depends on the diffusion of molecules, which mainly relies on the residence time or flow velocity of fluid in the microchannel. Comparing Figure 5a with Figure 5d, the velocity profiles in fluid field are displayed via the streamline. The fluid state can be considered as laminar flow at $Re = 1$. In this case, the residence time of fluid is almost equal on account of similar structures for the two micromixers. Besides, the secondary flow is weak extremely in this condition. Consequently, negligible difference appears between two velocity fields.

With the increase of the Reynolds number, the advantages of the modified structure are amplified gradually. In Figure 5e, when the Reynolds number is increased to 50 in the novel micromixer, the velocity profile has changed dramatically compared with that shown in Figure 5b. Attributed to the asymmetry of lateral wall structure, two complete vortexes with round shape in the upper velocity profile become clearly visible, whereas the vortex in Figure 5b is closer to ellipse shape. Moreover, the increasing velocity strengthens the inertia effect of fluid, and the mixing time will be shortened especially for the fluid around the sectional centerline of the microchannel. On the other hand, because of the promoted fluid velocity after converging wall with high curl, the more residence time and longer mixing distance in the novel micromixer may be available due to the formation of more concentrated vortex, compared with the ordinary "S"-shaped structure. In a word, fluid velocity acceleration in the

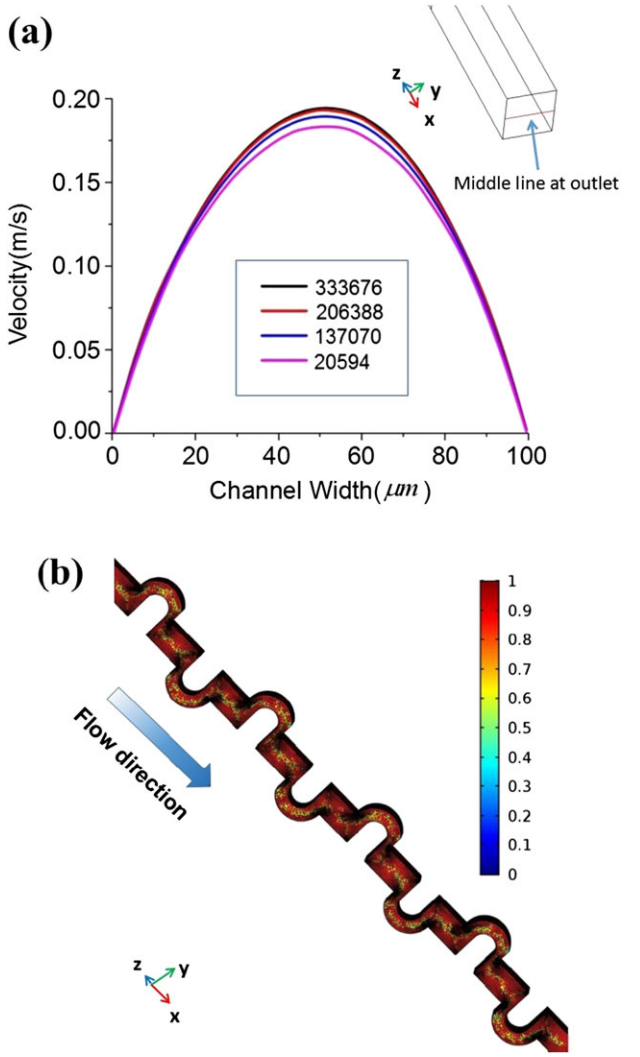

FIGURE 3 (a) The local velocity profiles along the middle line at outlet. (b) The mesh system with 206,388 elements; the color legend varies on behalf of the quality of elements

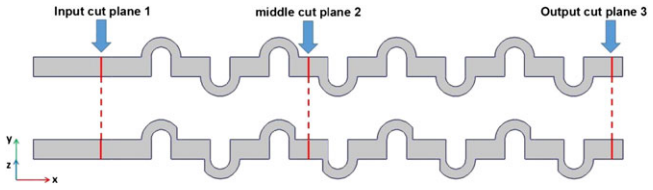

FIGURE 4 The aerial view of channel and the location distribution of cut planes in two micromixers

modified lateral wall structure becomes more significant than that in the "S"-shaped microchannel. Therefore, the flow field in the former tends to be subjected to larger disturbances than the latter, which will be dedicated to the improvement of mixing performance inevitably. The precisely numerical simulation has verified this result, and the specific value can be derived from the color legend.

When the Reynolds number increases to 100, the flow rate is higher significantly and the secondary flow gets to be more distinct in the modified path than that in the "S"-shaped microchannel, as shown in Figure 5c with Figure 5f. Besides, it can be seen that the center of the vortex gets closer to two sides of the microchannel. At the same time, the vortex maintains more complete configuration in Figure 5f in comparison with that in Figure 5c. In some sense, it means that as the flow rate increases, the intensity of the secondary flow in the novel path will be also on the rise. In general, the converging wall structure is inclined to accelerate and maintain vortex strength at the relatively high flow rate and further elevate the mixing efficiency of the micromixer. It is worth mentioning that these sequence diagrams of Figure 5 are equipped with different velocity profiles as demonstrated as the color legend beneath.

3.2 | Concentration distribution and the mixing performance

For obtaining in-depth information on varying mixing degree during the fluid flow at different Reynolds number, the concentration profile could be objective to the evaluation comprehensively.

Three concentration slices parallel to the y–z plane are selected to show the distribution of fluid concentration, which are located at the inlet, the middle, and the outlet positions of the pipeline, respectively, as illustrated in Figure 4. Although fluid flows into the entrance in parallel with the divisional interface, there is only tiny molecular diffusion flux happening between two kinds of reagents before flowing into the curved path as shown in Cut Plane 1 in Figure 6. After passing through a few lateral structures, fluid reaches Cut Plane 2, molecular diffusion occurs clearly and similarly at the interface of reagents as shown in A_{12} and B_{12}, considering the low velocity and weak convection when the Reynolds number is equal to 1. As the Reynolds number increases to 10, as shown in A_{22} and B_{22}, the fluid with high concentration is expanded gradually into the fluid with low concentration, and the fluid in lateral wall microchannel is stretched along the centerline of section to enlarge the contact area between the reagents. A stronger secondary flow gets to be generated when the Reynolds number increases to 50; the fluid with high concentration still maintains a large proportion in A_{32}, but in B_{32}, the proportion of fluid with high concentration is reduced markedly due to the vortex rotating and stirring the fluid field continuously. When the Reynolds number increases to 100, there are still a few of the fluid with high concentration appearing in section of "S"-shaped micromixer as shown in A_{42}. By contrast, the fluctuating range of the

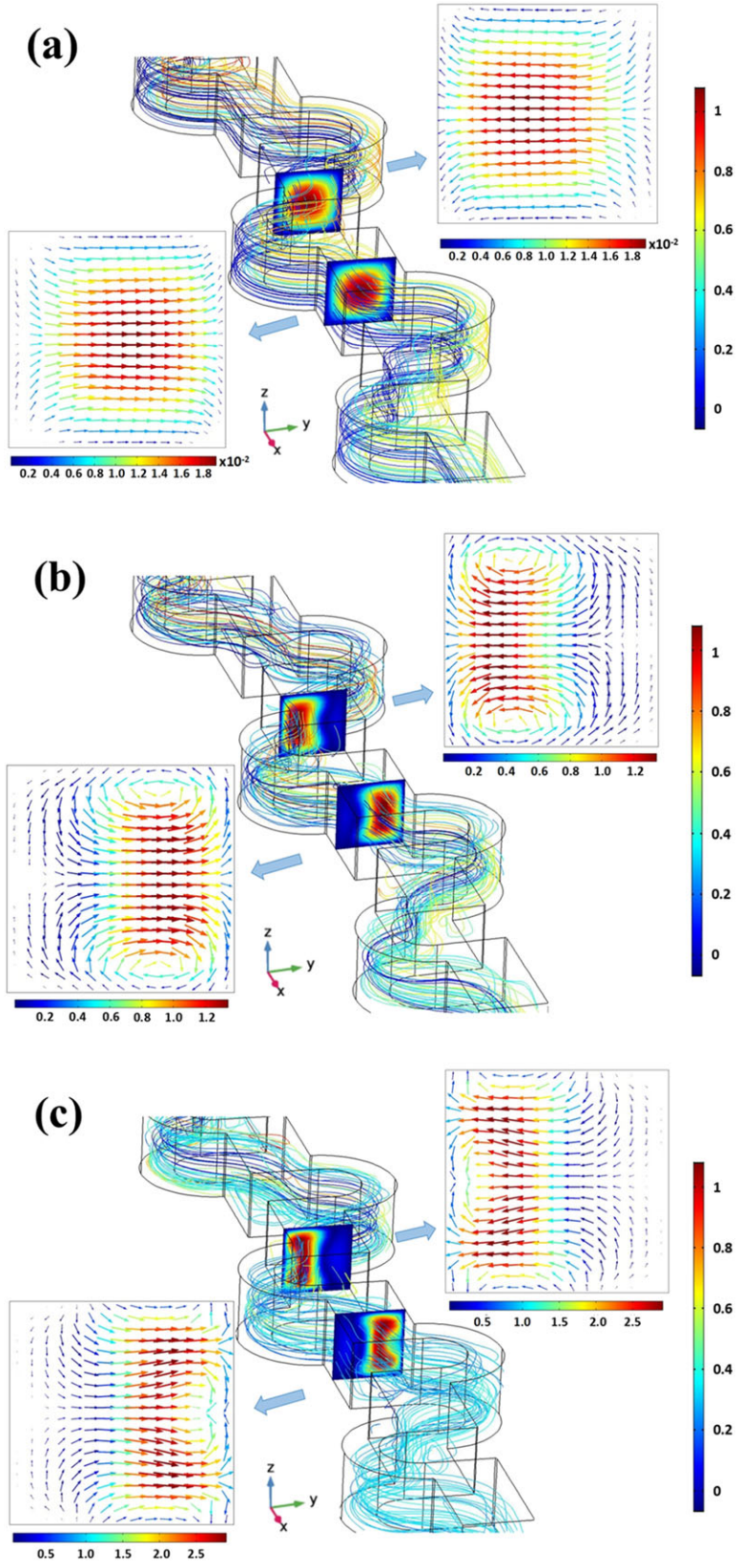

FIGURE 5 The mixing performance of two micromixers under different Re with the concentration distribution shown in the color legend at the right side; the windows distributed on both sides of the microchannel illustrate the local velocity fields of vertical sections, and the color legends beneath indicate the velocity magnitude (m/s). (a) The "S"-shaped micromixer at Re = 1; (b) the "S"-shaped micromixer at Re = 50; (c) the "S"-shaped micromixer at Re = 100; (d) the micromixer with modified lateral wall at Re = 1; (e) the micromixer with modified lateral wall at Re = 50; (f) the micromixer with modified lateral wall at Re = 100

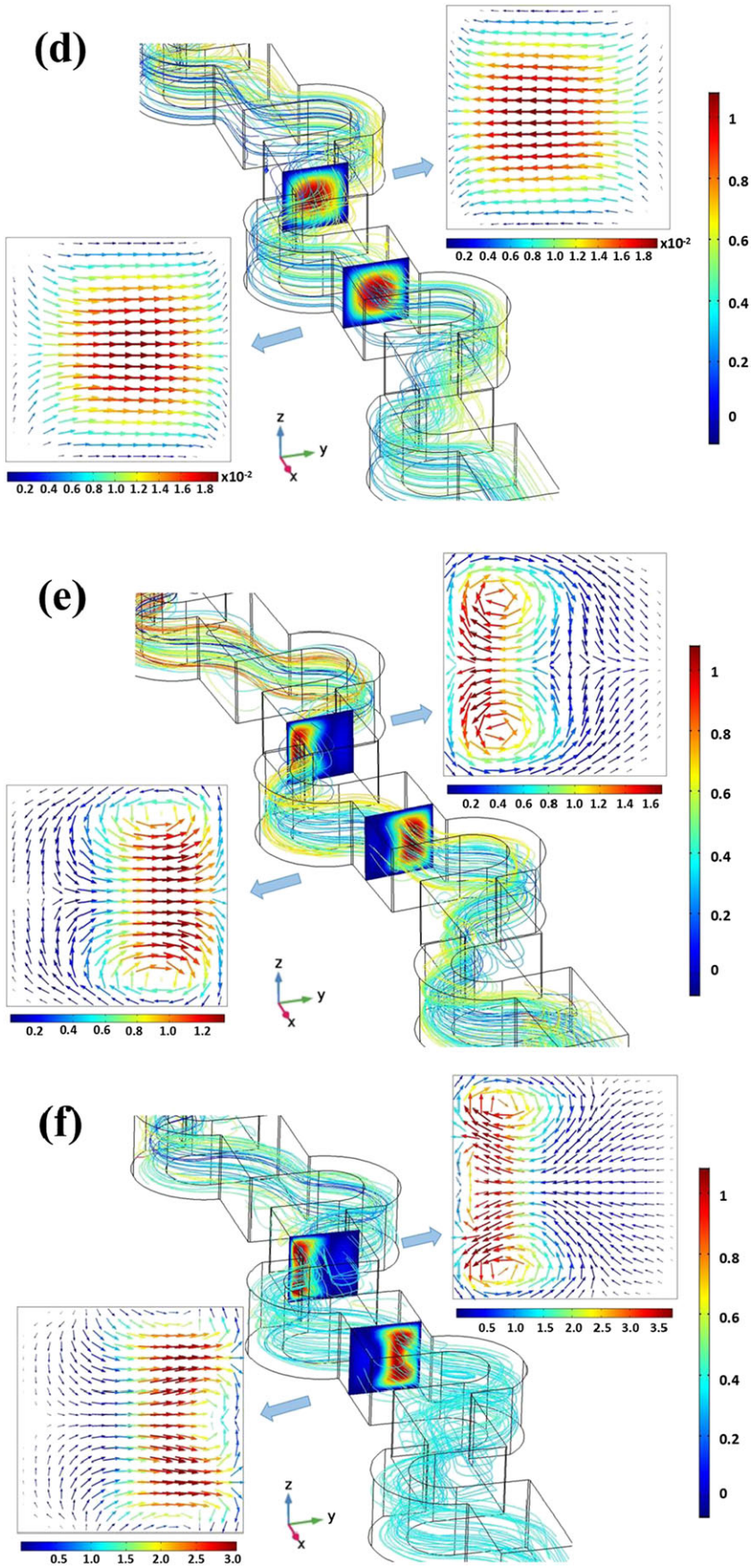

FIGURE 5 Continued

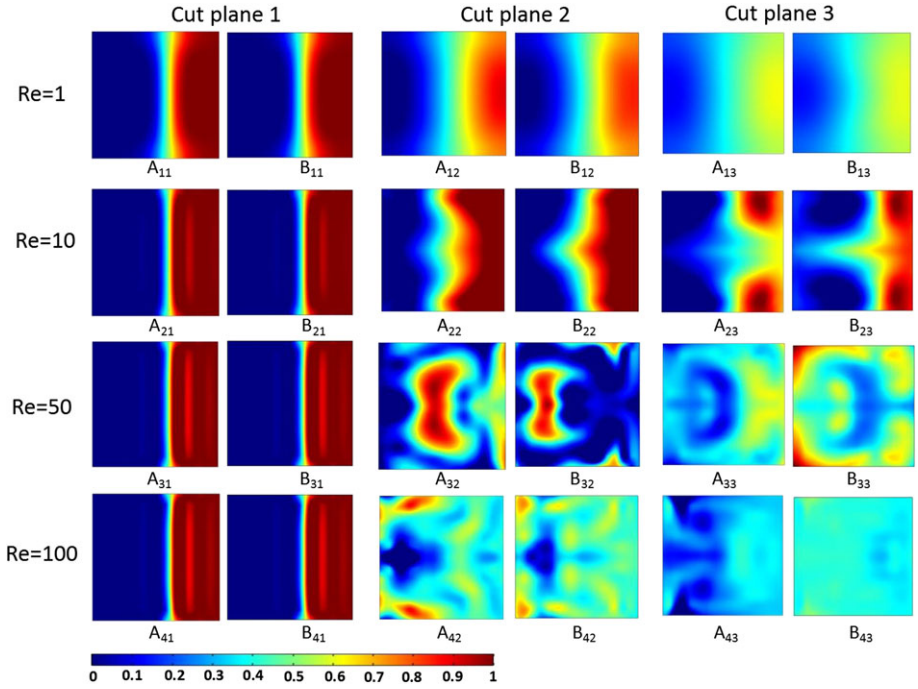

FIGURE 6 The concentration distribution of fluid in three cut planes as Re varies, where A_{ij} and B_{ij} represent the plane serial numbers. (A and B stand for "S"-shaped micromixer and the micromixer with modified lateral wall, respectively. The subscript i represents four types of Re, and the subscript j represents cut planes at three positions as shown in Figure 4; the color legend represents the concentration distribution ranging from 0 to 1)

concentration distribution is relatively narrow with its mean value close to 0.5 in B_{42}. Similar conclusion can also be obtained from the concentration distribution at Cut Plane 3, as shown in A_{13}–A_{43} and B_{13}–B_{43}. It is worth mentioning that when the Reynolds number reaches to 100, the fluid concentration distribution achieves a fairly high uniformity degree in the novel micromixer as shown in B_{43}, whereas there is still a quite large proportion of fluid with low concentration remained in the "S"-shaped micromixer as shown in A_{43}.

To demonstrate those concentration diversities along the central axis during the process of fluid flow, we also provide the concentration distribution profiles in the longitudinal section in parallel to the *x*–*y* flat, and its position is just in the middle of the length in the *z* direction, as shown in Figure 7. As demonstrated from these concentration slices, with increasing Reynolds number, mixing effect is also increasing gradually due to the enhanced convection effect and the secondary flow between reagents, which dominate the improvement of the mixing performance eventually. Moreover, the acceleration effect in fluid flow brought by the modified structure may also play a very effective role in the process of mixing; thus, the convection effect between reagents is enlarged, which will benefit to obtain better mixing performance. That means, for achieving the expected mixing degree, less length of

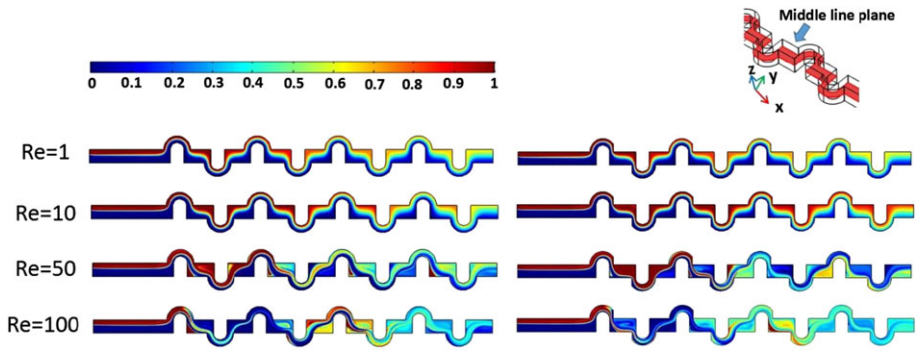

FIGURE 7 The concentration distribution profiles in the longitudinal section for two micromixers at different Re. The left four profiles are for the ordinary "S"-shaped structure, and the others are for the novel structure. The color legend represents the concentration range from 0 to 1. The minimap at the upper right corner demonstrates the position of the longitudinal section

micropaths should be required for the novel structure in contrast with the ordinary structure. In other words, the former may be more efficient than the latter for promotion of mixing performance.

To investigate the output uniformity of fluid after a process of mixing, the mixing index M is proposed in the above section and its dependence on different Re at the outlet position for two micromixers is obtained via postprocessing techniques of numerical calculation. As shown in Figure 8, compared with the ordinary "S"-shaped structure of the micromixer, the promotion of mixing index in modified lateral wall microchannel is not quite remarkable in the condition of the Reynolds number lower than 10. However, as the Reynolds number is above 30, the mixing index in modified lateral wall microchannel achieves an overall dominance on the ordinary "S"-shaped structure. Specifically, the mixing index in "S"-shaped microchannel is less than 30% at Re = 30, whereas the mixing index can arrive to 55% in modified structure, which means a tremendous elevation of fluid mixing degree. Furthermore, for the "S"-shaped microchannel, the mixing index ascends to a peak value at Re = 50 and then follows a rapid decrease as Reynolds number increased to 100, which has violated the original intention of the structure design of micromixer. On the other hand, the mixing index in the modified lateral microchannel maintains a general increasing trend while the Reynolds number is beyond 10. Especially, the mixing index achieves a maximum value of 80% approximately at Re = 100, a leading superiority of about 40% over the ordinary structure. Therefore, we believe that this novel micromixer should possess a better mixing performance and higher efficiency than the "S"-shaped microchannel on the condition of appropriate arrangement of lateral wall structure.

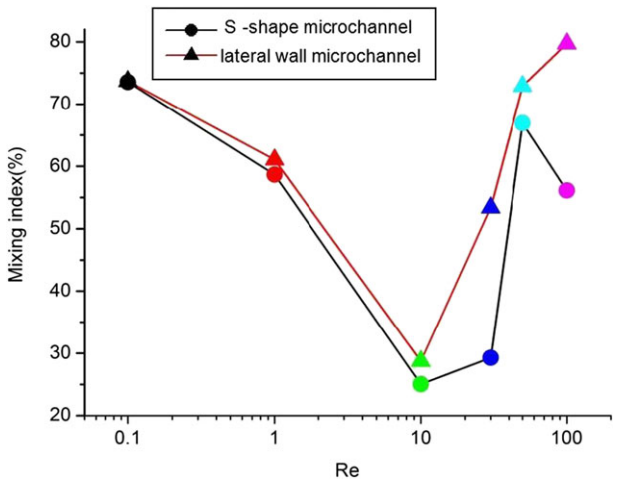

FIGURE 8 The dependence of mixing index on different Re at the outlet position for two micromixers. The outlet position has been illustrated in Figure 3

4 | CONCLUSIONS

In this study, a novel passive micromixer is designed based on asymmetric lateral wall structures and the secondary flow. By a large number of numerical calculations and comparative analysis on the common traits and differences of fluid flow between the novel micromixer and the "S"-shaped channel, some meaningful conclusions can be drawn:

1. Although Reynolds number ranges from 30 to 100, because of the formation of the secondary flow and increasing inertial effect, fluid velocity acceleration in the modified lateral wall structure becomes more significant than that in the "S"-shaped microchannel, which tends to bring about larger disturbances in the flow field of novel micromixer and further leads to the improvement of its mixing performance.
2. With increasing Reynolds number, mixing effect is also increasing gradually due to the enhanced convection effect and the secondary flow between reagents. When the Reynolds number reaches to 100, the fluid concentration distribution achieves a fairly high uniformity degree in the novel micromixer; whereas there is still a quite large proportion of fluid with low concentration remained in the "S"-shaped micromixer.
3. On the condition that the Reynolds number is lower than 10, the promotion of mixing index in modified lateral wall microchannel is not quite remarkable in comparison with the ordinary "S"-shaped structure. However, although the Reynolds number is above 30, the mixing index in modified lateral wall microchannel achieves an overall dominance on the ordinary "S"-shaped structure, which approves the better mixing performance and higher efficiency of the novel micromixer.

According to its superior mixing performance, we believe that this novel micromixer should have a potential application prospects in the premise that its mixing reliable is verified by experiment results in the further research works.

ACKNOWLEDGEMENTS

This research was is funded by National Natural Science Foundation of China (Grant 51605124), Youth Fund of Hainan University (hdkyxj201721 and hdkyxj201722), and the Open Research Project of the State Key Laboratory of Industrial Control Technology, Zhejiang University, China (ICT170295).

CONFLICTS OF INTEREST

The authors declare no conflicts of interest.

ORCID

Liuyong Shi http://orcid.org/0000-0002-1412-4237
Teng Zhou http://orcid.org/0000-0002-8744-9083

REFERENCES

1. Whitesides GM. The origins and the future of microfluidics. *Nature*. 2006;442(7101):368-373.
2. Demello AJ. Control and detection of chemical reactions in microfluidic systems. *Nature*. 2006;442(7101):394-402.
3. Rajabi N, Bahnemann J, Tzeng TN, Barradas OP, Zeng AP, Müller J. Lab-on-a-chip for cell perturbation, lysis, and efficient separation of sub-cellular components in a continuous flow mode. *Sensor Actuat A-Phys*. 2014;215(16):136-143.
4. Zhou T, Liu ZY, Wu YH, Deng YB, Liu YS, Liu G, Hydrodynamic particle focusing design using fluid-particle interaction, *Biomicrofluidics*, 2013,7 (5) :54104, 054104.
5. Zhou T, Ge J, Shi LY, Fan JQ, Liu ZY, Joo SW. Dielectrophoretic choking phenomenon of a deformable particle in a converging-diverging microchannel. *Electrophoresis*. 2018;39(4):590-596.
6. Liu X, Mwangi M, Li X, O'Brien M, Whitesides GM. Paper-based piezoresistive MEMS sensors. *Lab Chip*. 2011;11(13):2189-2196.
7. Deng YB, Wu YH, Xuan M, Korvink JG, Liu ZY., Dynamic optimization of valveless micropump, 16th International Solid-State Sensors, Actuators and Microsystems Conference, 2011:442–445.
8. Lee CY, Chang CL, Wang YN, Fu LM. Microfluidic mixing: a review. *Int J Mol Sci*. 2011;12(5):3263-3287.
9. Zhou T, Liu T, Deng YB, Chen LM, Qian SZ, Liu ZY. Design of microfluidic channel networks with specified output flow rates using the CFD-based optimization method. *Microfluid Nanofluid*. 2017;21(1):11.
10. Zhou T, Xu YF, Liu ZY, Joo SW. An enhanced one-layer passive microfluidic mixer with an optimized lateral structure with the dean effect. *J Fluid Eng-Tasme*. 2015;137(9):091102.
11. Yang AS, Chuang FC, Chen CK, et al. A high-performance micromixer using three-dimensional Tesla structures for bio-applications. *Chem Eng J*. 2015;263:444-451.
12. Zhou T, Wang HL, Shi LY, Liu ZY, Joo SW. An enhanced electroosmotic micromixer with an efficient asymmetric lateral structure. *Micromachines*. 2016;7(12):218.
13. Qian SZ, Bau HH. A chaotic electroosmotic stirrer. *Anal Chem*. 2002;74(15):3616-3625.
14. Yi MQ, Qian SZ, Bau HH. A magnetohydrodynamic chaotic stirrer. *J Fluid Mech*. 2002;468:153-177.
15. Qian SZ, Zhu JZ, Bau HH. A stirrer for magnetohydrodynamically controlled minute fluidic networks. *Phys Fluids*. 2002;14(10):3584-3592.
16. Qian SZ, Bau HH. Magneto-hydrodynamic stirrer for stationary and moving fluids. *Sens Actuators B*. 2005;106(2):859-870.
17. Qian SZ, Bau HH. Theoretical investigation of electro-osmotic flows and chaotic stirring in rectangular cavities. *App Math Model*. 2005;29(8):726-753.
18. Chen XY, Liu C, Xu Z, Pan YZ, Liu JS, Du LQ. An effective PDMS microfluidic chip for chemiluminescence detection of cobalt (II) in water. *Microsyst Technol*. 2013;19(1):99-103.
19. Liao Y, Song JX, Li E, et al. Rapid prototyping of three-dimensional microfluidic mixers in glass by femtosecond laser direct writing. *Lab Chip*. 2012;12(4):746-749.
20. Chen XY, Li TC. A novel design for passive misscromixers based on topology optimization method. *Biomed Microdevices*. 2016;18(4):1-15.
21. Hossain S, Ansari MA, Husain A, Kim KY. Analysis and optimization of a micromixer with a modified Tesla structure. *Chem Eng J*. 2010;158(2):305-314.
22. Goovaerts R, Smits W, Desmet G, Denayer J, Malsche WD. Combined improved mixing and reduced energy dissipation by combining convective effects and lamination. *Chem Eng J*. 2012;211:260-269.
23. Cosentino A, Madadi H, Vergara P, Vecchione R, Causa F, Netti PA. An efficient planar accordion-shaped micromixer: from biochemical mixing to biological application. *Sci rep-UK*. 2015;5:srep17876.
24. Chen XY, Zeng H, Wang H, Zhang D. Modeling, simulation and optimized design of a microreactor for a two-step reaction. *Chem Eng Technol*. 2013;36(4):591-595.
25. Chen XY, Shen JN, Hu ZL, Huo XY. Manufacturing methods and applications of membranes in microfluidics. *Biomed Microdevices*. 2016;18(6):104.
26. Chen XY, Liu C, Xu Z, Liu JS, Du LQ. Macro-micro modeling design in system-level and experiment for a micromixer. *Anal Methods-UK*. 2012;4(8):2334-2340.
27. Chen XY, Shen JN. Numerical analysis of mixing behaviors of two types of E-shape micromixers. *Int J Heat Mass Tran*. 2017;106:593-600.
28. Chen XY, Li TC, Zeng H, Hu ZL, Fu BD. Numerical and experimental investigation on micromixers with serpentine microchannels. *Int J Heat Mass Tran*. 2016;98:131-140.
29. Chen XY, Shen JN. Numerical and experimental investigation on splitting-and-recombination micromixer with E-shape mixing units. *Microsyst Technol*. 2017;23(10):4671-4677.
30. Chen XY, Zhang Z, Yi DL, Hu ZL. Numerical studies on different two-dimensional micromixers basing on a fractal-like tree network. *Microsyst Technol*. 2017;23(3):755-763.
31. Boonyasit Y, Maturos T, Sappat A, Jomphoak A, Tuantranont A, Laiwattanapaisal W. Passive micromixer integration with a microfluidic chip for calcium assay based on the arsenazo III method. *Biochip J*. 2011;5(1):1-7.
32. Chen XY, Wang XL. Optimized modular design and experiment for staggered herringbone chaotic micromixer. *Int J Chem React Eng*. 2015;13(3):305-309.
33. Viktorov V, Nimafar M. A novel generation of 3D SAR-based passive micromixer: efficient mixing and low pressure drop at a low Reynolds number. *J Micromech Microeng*. 2013;23(5):055023.

34. Lee CY, Wang WT, Liu CC, Fu LM. Passive mixers in microfluidic systems: a review. *Chem Eng J*. 2016;288:146-160.
35. Chen XY. Topology optimization of microfluidics—a review. *Microchem J*. 2016;127:52-61.
36. Liu YS, Deng YB, Zhang P, Liu ZY, Wu YH. Experimental investigation of passive micromixers conceptual design using the layout optimization method. *J Micromech Microeng*. 2013;23(7):75002-75011(10).
37. Pennella F, Rossi M, Ripandelli S, et al. Numerical and experimental characterization of a novel modular passive micromixer. *Biomed Microdevices*. 2012;14(5):849-862.
38. Afzal A, Kim KY. Multi-objective optimization of a passive micromixer based on periodic variation of velocity profile. *Chem Eng Commun*. 2015;202(3):322-331.
39. Ju J, Warrick J. Passive micromixer using by convection and surface tension effects with air-liquid interface. *Biochip J*. 2013;7(4):361-366.
40. Tseng LY, Yang AS, Lee CY, Hsieh CY. CFD-based optimization of a diamond-obstacles inserted micromixer with boundary protrusions. *Eng Appl Comp Fluid*. 2011;5(2):210-222.
41. Wang L, Ma SH, Han XJ. Micromixing enhancement in a novel passive mixer with symmetrical cylindrical grooves. *Asia-Pac J Chem Eng*. 2015;10(2):201-209.
42. Wang L, Ma SH, Wang XJ, Bi HM, Han XJ. Mixing enhancement of a passive microfluidic mixer containing triangle baffles. *Asia-Pac J Chem Eng*. 2014;9(6):877-885.
43. Afzal A, Kim KY. Passive split and recombination micromixer with convergent–divergent walls. *Chem Eng J*. 2012;203:182-192.
44. Lim TW, Son Y, Jeong YJ, et al. Three-dimensionally crossing manifold micro-mixer for fast mixing in a short channel length. *Lab Chip*. 2011;11(1):100-103.
45. Guo YC, Xu YF, Deng YB, Liu ZY. Topology optimization of passive micromixers based on Lagrangian mapping method. *Micromachines*. 2018;9(3):137.
46. Deng YB, Liu ZY, Zhang P, Liu YS, Gao QY, Wu YH. A flexible layout design method for passive micromixers. *Biomed Microdevices*. 2012;14(5):929-945.
47. Gobby D, Angeli P, Gavriilidis A. Mixing characteristics of T-type microfluidic mixers. *J Micromech Microeng*. 2001;11(2):126-132.
48. Zhang YR, Hu YD, Wu HY. Design and simulation of passive micromixers based on capillary. *Microfluid Nanofluid*. 2012;13(5):809-818.
49. Alam A, Kim KY. Analysis of mixing in a curved microchannel with rectangulars grooves. *Chem Eng J*. 2012;181:708-716.
50. Chen XY, Shen JN. Review of membranes in microfluidics. *J Chem Technol Biotechnol*. 2017;92(2):271-282.
51. Chen XY, Li TC, Hu ZL. A novel research on serpentine microchannels of passive micromixers. *Microsyst Technol*. 2016;23:1-8.

How to cite this article: Wang H, Shi L, Zhou T, Xu C, Deng Y. A novel passive micromixer with modified asymmetric lateral wall structures. *Asia-Pac J Chem Eng*. 2018;13:e2202. https://doi.org/10.1002/apj.2202